

Surface Structure and Electronic Properties of $\text{Lu}_3\text{Al}_5\text{O}_{12}$

Weian Guo ^{1,2}, Benxue Jiang ^{1,*}, Jiajie Zhu ³ and Long Zhang ^{1,*}

¹ Key Laboratory of Materials for High Power Laser, Shanghai Institute of Optics and Fine Mechanics, Chinese Academy of Sciences, Shanghai 201800, China; weianguo@siom.ac.cn

² Center of Materials Science and Optoelectronics Engineering, University of Chinese Academy of Sciences, Beijing 100049, China

³ Department of Physics, Tongji University, Shanghai 200092, China; zhujiatie@163.com

* Correspondence: jiangsic@foxmail.com (B.J.); longzhang@siom.ac.cn (L.Z.)

Abstract: $\text{Lu}_3\text{Al}_5\text{O}_{12}$ (LuAG) is a famous scintillator that has the advantages of high efficiency, high light yield, and fast decay after being doped with active ions. F centers (oxygen vacancies with two electrons) and antisite defects are the most important defects and can greatly affect the scintillation performance in the bulk materials. However, the surface defects that strongly affect the spectrum of a single crystal (SC) and single crystal film (SCF) and the effect on the electronic properties have not been investigated. In this context, we investigate the surface structural and electronic properties of $\text{Lu}_3\text{Al}_5\text{O}_{12}$ using first-principles calculations. The Lu atoms are six-fold and seven-fold coordinated with the O atoms on the S1 and S2 surfaces. The surface oxygen vacancies and antisites have considerably lower formation energies than for the bulk. The oxygen vacancies in the bulk introduce the occupied states in the band gap. The surface electronic states are mainly located on the oxygen atoms and can be eliminated via oxygen vacancies.

Keywords: $\text{Lu}_3\text{Al}_5\text{O}_{12}$; scintillation; surface defect; electronic properties



Citation: Guo, W.; Jiang, B.; Zhu, J.; Zhang, L. Surface Structure and Electronic Properties of $\text{Lu}_3\text{Al}_5\text{O}_{12}$. *Crystals* **2021**, *11*, 1433. <https://doi.org/10.3390/cryst11111433>

Academic Editors: Jung-Yeol Yeom, David Stratos and Ioannis Kandarakis

Received: 30 September 2021
Accepted: 2 November 2021
Published: 22 November 2021

Publisher's Note: MDPI stays neutral with regard to jurisdictional claims in published maps and institutional affiliations.



Copyright: © 2021 by the authors. Licensee MDPI, Basel, Switzerland. This article is an open access article distributed under the terms and conditions of the Creative Commons Attribution (CC BY) license (<https://creativecommons.org/licenses/by/4.0/>).

1. Introduction

The garnet ($\text{A}_3\text{B}_5\text{O}_{12}$) single crystal is a type of material that has been widely used in photonics for a long time [1–4] and its scintillation characteristics are currently being investigated because of a demand in the detection system [5,6]. Moszynski first characterized the scintillation performance of $\text{Y}_3\text{Al}_5\text{O}_{12}$ (YAG) [7]. With respect to YAG, LuAG doped with Ce ions has a relatively high density (6.73 g/cm^3) and the scintillation efficiency is 7 or 8 times than that of BGO ($\text{Bi}_4\text{Ge}_3\text{O}_{12}$) [8]. However, the light yield and decay time of LuAG is 3 times [9] and one fifth of that of BGO [10,11] respectively, once doped with active ions. However, there are many “traps” in the lattice of LuAG which can cause lead to slow components by capturing carriers in transport processing [12]. Nikl [13] highlighted that the most important defects in garnet scintillation crystals are its antisite defects. Systematic studies [12] revealed that the antisite defects acted as shallow traps in LuAG single crystals, which is attributed to the performance degradation by introducing defect energy levels in the gap. Kuklja [14] investigated all the possible defects of YAG and proved that among all types of defects, the most dominant is the Y_{Al} . Chen [15] found that oxygen vacancies with different charge states are strongly related to a specific absorption peak. It is important to note that oxygen vacancies can be introduced by radiation and have three different charge states, which are related to the F center (the first is the electron F^+ center, the second is the electron F center and the third is the electrons F^- center) [16]. The F centers have been observed in a large range of inorganic materials, including alkali halides [16] and some oxides [17]. The F center absorption bands of $\text{Y}_3\text{Al}_5\text{O}_{12}$ have been confirmed using optical spectroscopy in the reference [18]. The F centers play a very important role in surface science where surface structural defects are strongly correlated to the properties of crystals [19]. Additionally, these oxygen vacancies can also induce the degradation of radiation hardness of the scintillators [20]. The intrinsic luminescence of such complex

oxides has been extensively studied in previous work [21–23]. These results showed that the Lu₃Al₅O₁₂ (LuAG) single crystal (SC) and single crystal film (SCF) are characterized by different concentrations of antisite defects (AD) and oxygen vacancies which leads to changes in their luminescence spectrum. The SC displays self-trapped exciton (STE) emissions that peaked at 4.74 eV and 4.95 eV and AD emissions that peaked at 3.72 and 3.70 eV. However, AD emissions are not observed for the SCF. The SCF exhibits a dependence of the STE emissions on the AD concentrations [22,23]. Although the AD concentration of the SCF is considered to be lower than in the SC due to surface reconstruction, a detailed experimental and theoretical investigation has yet to be performed. First-principles calculations have been demonstrated to successfully address the stability of different defects in scintillators [24,25]. We therefore study the surface structural and electronic properties of LuAG. The Lu atoms have varied coordination numbers for different surfaces. The formation energy of oxygen vacancies and antisites on the surface is lower than in the bulk. Oxygen vacancies also introduce some impurity states in the gap. Our research is fundamental to develop an understanding of the structural behavior of LuAG garnet materials and i guiding stabilization strategies.

2. Computational Methods

All of the energy and electronic calculations are carried out in the framework of the density functional theory with the projector augmented plane-wave method [26], as implemented in the Vienna ab initio simulation package [27]. The exchange-correlation potential is based on generalized gradient approximation as proposed by Perdew, Burke, and Ernzerhof [28]. The cut-off energy for the plane wave basis is set to 400 eV. The energy criteria is set to 10^{−6} eV in an iterative solution of the Kohn–Sham equation. The structures are relaxed until the residual force on each atom has decreased by less than 0.01 eV/Å. A 2 × 2 × 2 k-mesh is used for integration in the Brillouin zone.

The formation energy ΔH(D, q) of a defect in charge state q can be calculated using the following formula [29]:

$$\Delta H(D, q) = E(D, q) - E(\text{perfect}) + \sum n_i \mu_i + q(E_{\text{VBM}} + E_{\text{F}}) \quad (1)$$

where E(D, q) and E(perfect) are the total energies of the defective and perfect cells, n_i is the number of the atoms removed or added to the cell, and μ_i is the chemical potential of the corresponding atoms. E_F is the Fermi level and E_{VBM} is the valence band maximum. The chemical potentials of Lu, Al, O are subjected to the following:

$$3\mu_{\text{Lu}} + 5\mu_{\text{Al}} + 12\mu_{\text{O}} = E(\text{Lu}_3\text{Al}_5\text{O}_{12}) \quad (2)$$

$$2\mu_{\text{Lu}} + 3\mu_{\text{O}} \leq E(\text{Lu}_2\text{O}_3) \quad (3)$$

$$2\mu_{\text{Al}} + 3\mu_{\text{O}} \leq E(\text{Al}_2\text{O}_3) \quad (4)$$

3. Results and Discussion

The bulk structure of Lu₃Al₅O₁₂ is shown in Figure 1. The lattice constant of the cubic structure is calculated to be 11.87 Å, which is close to the experimental value of 11.906 Å [30]. Two surfaces terminated with different atomic layers, namely S1 and S2, are selected to investigate the structural properties of Lu₃Al₅O₁₂(001) (Figure 1). The LuO₈, AlO₄, and AlO₆ polyhedron are broken on the surface. The Lu atoms are six-fold and seven-fold and are coordinated with the O atoms on the S1 and S2 surfaces, respectively. The corresponding average Lu–O bond lengths are 2.26 Å and 2.28 Å, which is slightly shorter than the bulk value (2.32 Å) as presented in Table 1. The Al atoms are five-fold coordinated on the S1 surface and four/five-fold coordinated on the S2 surface as compared to being four-fold and six-fold coordinated in the bulk, respectively. The corresponding average bond distance is calculated to be 1.83 Å and 1.78/1.87 Å for the S1 and S2 surfaces.

The values are shown to be 1.76 Å and 1.92 Å for the bulk. The outermost O atoms move outward by 0.47 Å and 0.14 Å on the S1 and S2 surfaces after relaxation, respectively.

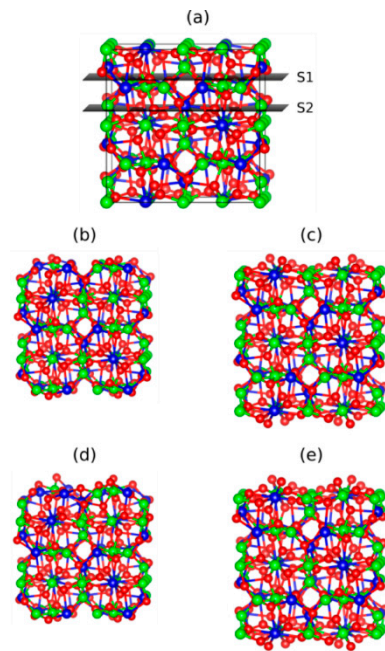


Figure 1. Structure of (a) optimized bulk $\text{Lu}_3\text{Al}_5\text{O}_{12}$ and unoptimized and optimized $\text{Lu}_3\text{Al}_5\text{O}_{12}(001)$ terminated with layer (b,d) S1 and (c,e) S2. The Lu, Al, and O atoms are shown in blue, green, and red.

Table 1. Calculated structural data of the Lu-O and Al-O bonding in the surface and bulk.

		Coordination	Length
Lu-O	S1	6	2.26 Å
	S2	7	2.28 Å
	bulk	8	2.32 Å
Al-O	S1	5	1.83 Å
	S2	4/5	1.78 Å/1.87 Å
	bulk	4/6	1.76 Å/1.92 Å

The total energies of nine and five oxygen vacancies on the S1 and S2 surfaces are compared in order to obtain the ground states. The formation energies are calculated to be -9.03 eV and -6.35 eV with reference to the bulk oxygen vacancy, reflecting more surface oxygen vacancies. The local structure near the vacant site for the ground states are shown in Figure 2. The bulk O atom is four-fold coordinated by two Lu atoms and two Al atoms with an average Lu-O and Al-O bond length of 2.33 Å and 1.84 Å, respectively. The surface O atom is only coordinated by two Lu atoms and one Al atom. The average Lu-O and Al-O bond length is calculated to be 2.16/2.26 Å and 1.90/1.87 Å, respectively, for the S1/S2 surface. The valence states are calculated to be +2.1 and +2.5, obtained using the Bader approach for the Lu and Al atoms in the bulk and on surface layers. The O atoms show a -1.2 valence state in the surface layer as compared to a -1.5 valence state in the bulk layer because of lack of the surrounding Al atom. Table 2 shows the calculated details.

On the other hand, the formation energies of the antisite defects on the S1 and S2 surfaces, namely the type of Lu_{Al} defect referred to in references [17–20], are calculated to be -2.16 eV and -2.09 eV with reference to the bulk antisites. The Lu atom prefers the six-fold and five-fold coordinated Al site in the bulk and on the surface, as illustrated in Figure 3. The average distances between the Lu atom and the neighboring O atoms are

calculated to be 2.14, 2.17, and 2.15 Å for the bulk, S1 surface, and S2 surface, respectively, which proves to be larger than in the perfect structure (1.76 Å and 1.92 Å) because of a smaller ionic radius of the Al than the Lu. The Al atoms are six-fold, five-fold, and six-fold coordinated by the O atoms in the bulk and on the S1 and S2 surfaces respectively, leading to bond lengths of 2.05, 1.90, 2.01 Å, which prove to be shorter than the value of 2.32 Å for the perfect lattice. Table 3 presents the details of the results.

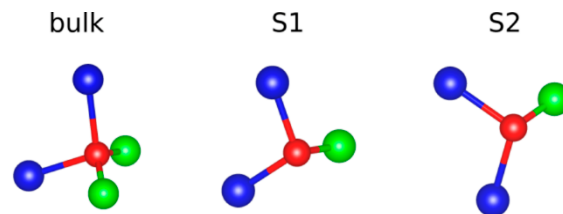


Figure 2. Local structure for the O vacant site in the bulk and on the surfaces. The Lu, Al, and O atoms are shown in blue, green, and red.

Table 2. The calculated structure and Bader charge state of O atom in the bulk and surface.

	Bulk O	S1 O	S2 O
Coordination	2Lu + 2Al	2Lu + 1Al	2Lu + 1Al
Lu-O	2.33 Å	2.16 Å	1.90 Å
Al-O	1.84 Å	2.26 Å	1.87 Å
Bader charge	−1.5		−1.2

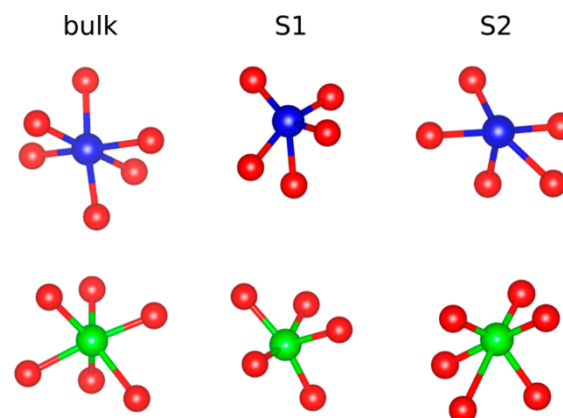


Figure 3. Local structure for the antisites (Lu_{Al}) in the bulk and on the surfaces. The Lu, Al, and O atoms are shown in blue, green, and red.

Figure 4 shows the total density of the states for the bulk and the surface without and with defects. The band gap of the bulk structure without defects is calculated to be 4.98 eV as compared to the experimental value of 8.2 eV [31]. Note that the DFT-PBE function usually underestimates the band gaps of semiconductors and insulators. The top of the valence band is primarily resultant of the O-2p states, while the bottom of the conduction band is composed of Lu-5d states, which is in good agreement with former theoretical results [30]. The oxygen vacancies introduced occupied states, containing two electrons that were located 2.32 eV above the valence band maximum because of weak binding, which is similar to the theoretical results for the oxygen vacancies in Lu_2SiO_5 [32]. No additional state appears in the gap for the antisites. The S1 surface displays some empty states at 0.16, 0.82, and 1.44 eV, containing 4, 10, and 2 holes. The holes are located at 0.17 (5 holes), and 0.66 (9 holes) eV for the surface with an oxygen vacancy, which releases two electrons and fills the holes. The antisites introduce holes at 0.12 (3 holes) and 0.91

(13 holes) eV. The S2 surface without and with the antisites reveal unoccupied states at 0.29 eV (12 holes) and 0.11/0.40 eV (1/11 holes). The extra states then shift to 0.08 (1 holes), 0.12 (5 holes), and 0.20 (4 holes) eV.

Table 3. The calculated structure data of antisite defects Lu_{Al} and Al atoms.

		Coordination	Length
LuAl-O	Bulk	6	2.14 Å
	S1	5	2.17 Å
	S2	5	2.15 Å
Al-O	Bulk	6	2.05 Å
	S1	5	1.90 Å
	S2	6	2.01 Å

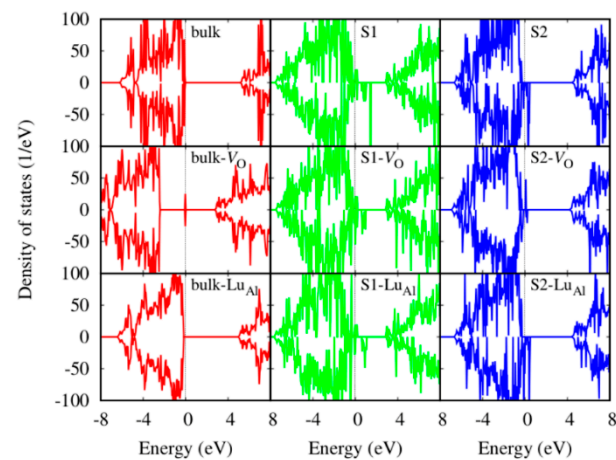


Figure 4. Density of states for the bulk and surfaces without and with defects. The Fermi energy level is set to zero.

The spatial distribution of the surface and defect states are illustrated in Figure 5. The electrons are located near the vacant site for the bulk with oxygen vacancies. The surface states are mainly contributed to by the holes on oxygen atoms because of the break of the Al-O and Lu-O bonds, which are for the most part, not influenced by the antisites. The introduction of oxygen vacancies eliminates some surface states due to the release of electrons.

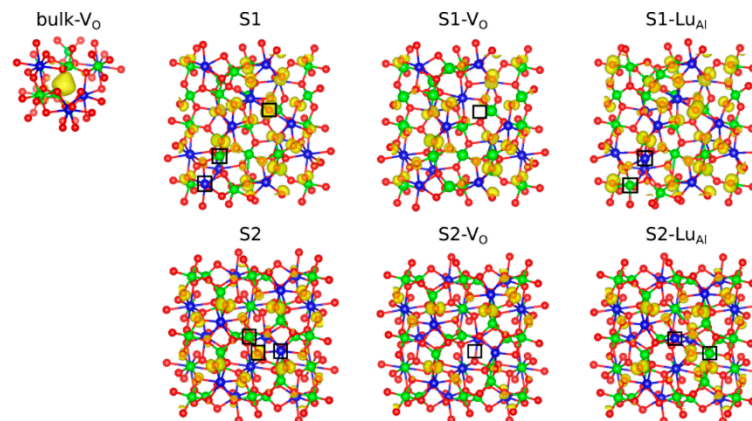


Figure 5. Projected charge density of the defect states in the band gap for the bulk and surfaces. The isovalue of the isosurfaces (yellow color) is set to 0.01 electrons/bohr³. The locations of the defect sites on the surface are marked by black squares.

4. Conclusions

The surface structure and electronic properties of $\text{Lu}_3\text{Al}_5\text{O}_{12}$ are investigated using first-principles calculations. The surface reconstruction leads to the outwards movement of the O atoms on the S1 and S2 surfaces, respectively. The oxygen vacancies and antisites have a higher concentration on the surface than in the bulk, which may lead to more intensive optical signals. Some extra states are introduced in the band gap because of the break of the Lu-O and Al-O bonds on the surfaces. The oxygen vacancies eliminate some of the unoccupied states, whereas the antisites have almost no effect.

Author Contributions: Conceptualization, W.G. and J.Z.; methodology, W.G. and J.Z.; software, W.G.; validation, J.Z. and B.J.; formal analysis, J.Z.; investigation, W.G. and J.Z.; resources, B.J. and L.Z.; data curation, J.Z.; writing—original draft preparation, W.G.; writing—review and editing, J.Z. and B.J.; visualization, W.G. and J.Z.; supervision, B.J. and J.Z.; project administration, B.J.; funding acquisition, B.J. and L.Z. All authors have read and agreed to the published version of the manuscript.

Funding: This research received no external funding.

Conflicts of Interest: The authors declare no conflict of interest.

References

1. Mao, J.; Wang, C.; Hong, T.; Yu, Y. Three-nanosecond-equal interval sub-pulse Nd: YAG laser with multi-step active Q-switching. *Chin. Opt. Lett.* **2021**, *19*, 071404. [[CrossRef](#)]
2. Tang, K.; Liao, W.; Lin, D.; Li, B.; Chen, W. Self-polarization emission based on coherent combination of intracavity eigenmodes in Nd:YAG/Cr⁴⁺:YAG lasers. *Chin. Opt. Lett.* **2021**, *19*, 3–7. [[CrossRef](#)]
3. Wei, M.; Cheng, T.; Dou, R.; Zhang, Q.; Jiang, H. Superior performance of a 2 kHz pulse Nd: YAG laser based on a gradient-doped crystal. *Photonics Res.* **2021**, *9*, 1191–1196. [[CrossRef](#)]
4. Sipes, D.L. Highly efficient neodymium: Yttrium aluminum garnet laser end pumped by a semiconductor laser array. *Appl. Phys. Lett.* **1985**, *47*, 74–75. [[CrossRef](#)]
5. Takayuki YANAGIDA Inorganic scintillating materials and scintillation detectors. *Proc. Jpn. Acad. Ser. B* **2018**, *94*, 75–97. [[CrossRef](#)]
6. Dujardin, C.; Auffray, E.; Bourret-Courchesne, E.; Dorenbos, P.; Lecoq, P.; Nikl, M.; Vasil'Ev, A.N.; Yoshikawa, A.; Zhu, R.Y. Needs, trends, and advances in inorganic scintillators. *IEEE Trans. Nucl. Sci.* **2018**, *65*, 1977–1997. [[CrossRef](#)]
7. Wolski, D. Properties of the YAG: Ce scintillator. *Nucl. Instrum. Methods Phys. Res. Sect. A Accel. Spectrometers Detect. Assoc. Equip.* **1994**, *345*, 461–467. [[CrossRef](#)]
8. Nikl, M. Energy transfer phenomena in the luminescence of wide band-gap scintillators. *Phys. Stat. Sol.* **2005**, *202*, 201–206. [[CrossRef](#)]
9. Nikl, M. Scintillation detectors for X-rays. *Meas. Sci. Technol.* **2006**, *17*, 37–54. [[CrossRef](#)]
10. Gironnet, J.; Mikhailik, V.B.; Kraus, H.; Marcillac, P.; De Coron, N. Scintillation studies of $\text{Bi}_4\text{Ge}_3\text{O}_{12}$ (BGO) down to a temperature of 6 K. *Nucl. Instrum. Methods Phys. Res. Sect. A Accel. Spectrometers Detect. Assoc. Equip.* **2008**, *594*, 358–361. [[CrossRef](#)]
11. Nikl, M.; Yoshikawa, A.; Kamada, K.; Nejezchleb, K. Development of luag-based scintillator crystals—A review. *Prog. Cryst. Growth Charact. Mater.* **2013**, *59*, 47–72. [[CrossRef](#)]
12. Nikl, M.; Vedda, A.; Fasoli, M.; Fontana, I.; Laguta, V.V.; Mihokova, E.; Pejchal, J.; Rosa, J.; Nejezchleb, K. shallow traps and radiative recombination processes in $\text{lu}_3\text{al}_5\text{o}_{12}$: Ce single crystal scintillator. *Phys. Rev. B* **2007**, *76*, 195121. [[CrossRef](#)]
13. Nikl, M.; Laguta, V.V.; Vedda, A. Complex oxide scintillators: Material defects and scintillation performance. *Phys. Status Solidi B* **2008**, *245*, 1701–1722. [[CrossRef](#)]
14. Kuklja, M.M. Defects in yttrium aluminium perovskite and garnet crystals: Atomistic study. *J. Phys. Condens. Matter* **2000**, *12*, 2953–2967. [[CrossRef](#)]
15. Chen, J.; Lu, T.C.; Xu, Y.; Xu, A.G.; Chen, D.Q. Ab initio study of a charged vacancy in yttrium aluminum garnet ($\text{Y}_3\text{Al}_5\text{O}_{12}$). *J. Phys. Condens. Matter* **2008**, *20*, 325212. [[CrossRef](#)]
16. Popov, A.I.; Kotomin, E.A.; Maier, J. Basic properties of the F⁻ type centers in halides, oxides and perovskites. *Nucl. Inst. Methods Phys. Res. B* **2010**, *268*, 3084–3089. [[CrossRef](#)]
17. Kotomin, E.A.; Popov, A.I. Radiation-induced point defects in simple oxides. *Nucl. Inst. Methods Phys. Res. B* **1998**, *141*, 1–15. [[CrossRef](#)]
18. Springis, M.; Pujats, A.; Valbis, J. Polarization of luminescence of colour centres in YAG crystals. *J. Phys. Condens. Matter* **1991**, *3*, 5457–5461. [[CrossRef](#)]
19. Sun, Y.; Egawa, T.; Shao, C.; Zhang, L.; Yao, X. Quantitative study of F center in high-surface-area anatase titania nanoparticles prepared by MOCVD. *J. Phys. Chem. Solids* **2004**, *65*, 1793–1797. [[CrossRef](#)]
20. Lushchik, A.; Lushchik, C.; Popov, A.I.; Schwartz, K.; Shablonin, E.; Vasil'chenko, E. Influence of complex impurity centres on radiation damage in wide-gap metal oxides. *Nucl. Inst. Methods Phys. Res. B* **2016**, *374*, 90–96. [[CrossRef](#)]

21. Babin, V.; Blazek, K.; Krasnikov, A.; Nejezchleb, K.; Nikl, M.; Savikhina, T.; Zazubovich, S. Luminescence of undoped LuAG and YAG crystals. *Phys. Status Solidi C*. **2005**, *2*, 97–100. [[CrossRef](#)]
22. Zorenko, Y.; Voloshinovskii, A.; Savchyn, V.; Voznyak, T.; Nikl, M.; Nejezchleb, K.; Mikhailin, V.; Kolobanov, V.; Spassky, D. Exciton and antisite defect-related luminescence in $\text{Lu}_3\text{Al}_5\text{O}_{12}$ and $\text{Y}_3\text{Al}_5\text{O}_{12}$ garnets. *Phys. Status Solidi B*. **2007**, *244*, 2180–2189. [[CrossRef](#)]
23. Voznyak, T.; Gorbenko, V.; Zorenko, T.; Voloshinovskii, A.; Vistovsky, V.; Nikl, M.; Nejezchleb, K.; Kolobanov, V.; Spasski, D. Luminescence Spectroscopy of Excitons and Antisite Defects in $\text{Lu}_3\text{Al}_5\text{O}_{12}$ Single Crystals and Single-Crystal Films. *Opt. Spectrosc.* **2008**, *104*, 75–87. [[CrossRef](#)]
24. Marinopoulos, A.G. First-principles study of the formation energies and positron lifetimes of vacancies in the Yttrium-Aluminum Garnet $\text{Y}_3\text{Al}_5\text{O}_{12}$. *Eur. Phys. J. B* **2019**, *92*, 3–9. [[CrossRef](#)]
25. Jia, Y.; Miglio, A.; Gonze, X.; Mikami, M. Ab-initio study of oxygen vacancy stability in bulk and Cerium-doped lutetium oxyorthosilicate. *J. Lumin.* **2018**, *204*, 499–505. [[CrossRef](#)]
26. Blöchl, P.E. Projector augmented-wave method. *Phys. Rev. B* **1994**, *50*, 17953–17979. [[CrossRef](#)]
27. Joubert, D. From ultrasoft pseudopotentials to the projector augmented-wave method. *Phys. Rev. B* **1999**, *59*, 1758–1775. [[CrossRef](#)]
28. Perdew, J.P.; Burke, K.; Ernzerhof, M. Generalized gradient approximation made simple. *Phys. Rev. Lett.* **1996**, *77*, 3865–3868. [[CrossRef](#)] [[PubMed](#)]
29. Zhu, J.; Sidletskiy, O.; Boyaryntseva, Y.; Grynyov, B. Structure and role of carbon-related defects in yttrium aluminum garnet. *Opt. Mater.* **2021**, *111*, 110561. [[CrossRef](#)]
30. Hu, C.; Liu, S.; Shi, Y.; Kou, H.; Li, J.; Pan, Y.; Feng, X.; Liu, Q. Antisite defects in nonstoichiometric $\text{Lu}_3\text{Al}_5\text{O}_{12}$: Ce ceramic scintillators. *Phys. Status Solidi B* **2015**, *252*, 1993–1999. [[CrossRef](#)]
31. Zorenko, Y.; Zorenko, T.; Gorbenko, V.; Pavlyk, B.; Laguta, V.; Nikl, M.; Kolobanov, V.; Spassky, D. Luminescence and ESR characteristics of γ -irradiated $\text{Lu}_3\text{Al}_5\text{O}_{12}$:Ce single crystalline film scintillators. *Radiat. Meas.* **2010**, *45*, 419–421. [[CrossRef](#)]
32. Jia, Y.; Miglio, A.; Mikami, M.; Gonze, X. Ab initio study of luminescence in Ce-doped Lu_2SiO_5 : The role of oxygen vacancies on emission color and thermal quenching behavior. *Phys. Rev. Mater.* **2018**, *2*, 125202. [[CrossRef](#)]